The International Journal of Advanced Manufacturing Technology (2018) 98:2319–2333
https://doi.org/10.1007/s00170-018-2291-4

ORIGINAL ARTICLE

Effects of geometrical errors of guideways on the repeatability of positioning of linear axes of machine tools

Guangming Sun[1] · Gaiyun He[1] · Dawei Zhang[1] · Yicun Sang[1] · Xiaolei Zhang[1] · Bohui Ding[1]

Received: 20 January 2018 / Accepted: 4 June 2018 / Published online: 5 July 2018

Abstract

This paper studies the effects of geometrical errors on the repeatability of positioning of linear axes, based on theoretical modeling and an experimental study. Firstly, this paper elaborates on the mechanism of repeatability of positioning that is affected by motion pose of moving part. Secondly, a mathematical model is proposed between the geometrical error and motion pose of the moving part, based on point-by-point recursion. Subsequently, the influence of geometrical errors on the repeatability of positioning of the linear axes is obtained based on GA (genetic algorithm). Finally, the effectiveness of the proposed model is validated experimentally, and an assembly method for improving the repeatability of positioning is proposed. The method can provide designers and/or field engineers with informative guidelines for improving the repeatability of positioning in the design, manufacturing, and assembly processes.

Keywords Repeatability of positioning · Geometric error · Machine tools · Linear axes

1 Introduction

With the development of high-precision machine tools, higher repeatability of positioning is required [1–4]. Linear axe is one of the most important parts of multi-axis machine tools, and directly influences the final working accuracy of the tools [5–7]. The repeatability of positioning reflects the stability and consistency of the machine tool position and is an important indicator of machine tool performance [8]. At present, the mechanism of repeatability of positioning is not clear, and there is no effective method for guiding engineers to improve the repeatability of positioning of machine tools. An adjustment of the repeatability of positioning is a common but intractable problem in the machine tool assembly process, and mainly relies on the production experience of engineers, which bores much blindness, and provides low efficiency and poor consistency. As a matter of experience, the repeatability of positioning is affected by the assembly accuracy of guideways. Therefore, it is necessary to study the mechanism of assembly accuracy of guideway effects on the repeatability of positioning.

✉ Gaiyun He
hegaiyun@tju.edu.cn

[1] Key Laboratory of Mechanism Theory and Equipment Design of Ministry of Education, Tianjin University, Tianjin 300072, China

The assembly accuracy of guideways is determined by the assembly technique [9]. Over the past few decades, a considerable amount of intensive research has focused on machine tool assembly technique, and a series of measures has been put forward to improve assembly accuracy of machine tool [10, 11]. Guo et al. proposed a novel approach for measurement process planning in machine tool assembly by applying the observability principle of state space model, which provides designers with feasible measurement plans in assembly [12]. However, their work only focused on geometric errors of machine tool. Martin et al. proposed a method that allows an optimal adjustment of the machine tools in order to respect at best a set of standard functional requirements applied to a part [13]. However, their work considered only the tolerance. Guo et al. developed a state space model that integrates the geometric tolerance of components and variation propagation in assembly process to enhance assembly performance [14]. However, the elastic deformation was not taken into consideration. Sun et al. presented a pre-deformation machine center assembly method which considers the elastic deformation of machine tool [15]. He et al. proposed an approach to predicate the variation propagation considering elastic deformation in the assembly process of precision machine tools, and a pre-adjustment method in assembly design stage was proposed [16]. Ma presents an assembly error model of linear axis of CNC machine tool to analyze the effects of component

manufacturing error on axis considering component deformation [17]. However, their work has not analyzed the influence of the guideway geometric error on the motion error of table. Park proposed a transfer function method to develop a map of guideway geometrical error and table motion errors, and an adjustment method of guideway geometric error was proposed [18, 19]. Tang proposed an approach to calculate the straightness and angular errors based on measuring the guideway surface and fitting curve, the effectiveness of which was verified experimentally [20]. Majda proposed a FEA method for analyzing examination of the influence of geometric errors in a linear guideway on motion errors, and this approach aided in understanding and interpreting the results of experimental examinations of angular kinematic errors obtained for a real machine tool [21]. However, the works mentioned above are mainly focused on the effects of the geometrical errors on motion errors in linear axes; the relationship between the repeatability of positioning and the geometrical errors of guideways has not been studied.

This paper studies the mechanism of the geometric error effect on the repeatability of positioning based on the table motion pose and proposes an assembly method for improving the repeatability of positioning. The remainder of this paper is organized as follows. Section 2 addresses the mechanism of repeatability of positioning as affected by the table motion pose, an experiment is carried out to study the effect of motion pose on the positional deviation. Section 3 introduces the mathematical model comparing the geometrical errors and table motion pose based on point-by-point recursion. In this model, a force balance analysis of a table under geometrical errors of the guideways is first carried out. Then, an experiment is carried out to study the recovery of the elastic deformation of the slider component; the result shows that the elastic deformation is not fully recovered. Subsequently, the table motion pose at each position is calculated, which takes into account no-recovered elastic deformation, and the standard uncertainty of the table motion pose at each position is obtained. Finally, the optimal geometrical errors of the guideways are obtained based on the genetic algorithm. Section 4 analyzes the effects of geometrical errors of the guideways on the repeatability of positioning of linear axes. In Sect. 5, experiments are carried out in order to illustrate the effectiveness of the proposed model, and an assembly method for improving the repeatability of positioning is proposed. The conclusions are discussed in Sect. 6.

2 Mechanism of repeatability of positioning of linear axes based on table motion pose

Methods for evaluating the repeatability of positioning of linear axes are specified in ISO 230-2 [9]. The unidirectional repeatability of positioning in a given position can be expressed as

$$R_i\uparrow = 4S_i\uparrow \tag{1}$$

and

$$R_i\downarrow = 4S_i\downarrow \tag{2}$$

where the ↑ symbol signifies a parameter derived from a measurement made after an approach in the positive direction, and ↓ signifies that in the negative direction.

The bidirectional repeatability of positioning for a given position be expressed as

$$R_i = \max[2S_i\uparrow + 2S_i\downarrow + |B_i|; R_i\uparrow; R_i\downarrow] \tag{3}$$

where S_i denotes the standard uncertainty of the positioning deviations obtained through a series of n unidirectional approaches at position P_i, $S_i\uparrow = \sqrt{\frac{1}{n-1}\sum_{j=1}^{n}\left(X_{i,j}\uparrow - \overline{X}_i\uparrow\right)^2}$, $S_i\downarrow = \sqrt{\frac{1}{n-1}\sum_{j=1}^{n}\left(X_{i,j}\downarrow - \overline{X}_i\downarrow\right)^2}$; B_i denotes the reversal value at a given position, $B_i = \overline{X_i}\uparrow - \overline{X_i}\downarrow$; $X_{i,j}$ denotes the positional deviation, $X_{i,j} = P_{i,j} - P_i$; $\overline{X_{i,j}}$ denotes the mean unidirectional positional deviation, and $\overline{X}_i = \frac{1}{n}\sum_{j=1}^{n} X_{i,j}$.

A linear motion system consists of two guideways, four sliders, and a table. Six motion errors exist in the linear axes, including one positioning error, two straightness errors, and three angular errors, which determine the table motion pose, as shown in Fig. 1a. When the table moves to position i in jth time, its motion pose can be expressed as

$${}^{j}T_i = \left[{}^{j}\delta_{xx,i}\ {}^{j}\delta_{yx,i}\ {}^{j}\delta_{zx,i}\ {}^{j}\varepsilon_{xx,i}\ {}^{j}\varepsilon_{yx,i}\ {}^{j}\varepsilon_{zx,i}\right] \tag{4}$$

The positional deviation $X_{i,j}$ is affected by the table motion pose and can be expressed as follows:

$$X_{i,j} = {}^{j}\delta_{xx,i} + \left(l_h + {}^{j}\delta_{zx,i}\right){}^{j}\varepsilon_{yx,i} + \left(l_v + {}^{j}\delta_{yx,i}\right){}^{j}\varepsilon_{zx,i} + e_{L,i} \tag{5}$$

where l_h and l_v denote the distances between the test point and linear encoder in the horizontal and vertical directions, respectively. $e_{L,i}$ denotes the manufacturing error of linear encode, which is a constant in a constant temperature environment.

In order to study the effect of motion pose on the positional deviation of the table, an experiment was carried out on a horizontal machining tool in a constant temperature environment of 20 ± 0.5 °C, as shown in Fig. 2. A laser interferometer -Renishaw XM-60, which can measure the six motion errors of the table simultaneously, was used to measure the motion errors. The laser emitter was fixed on the table, and the laser

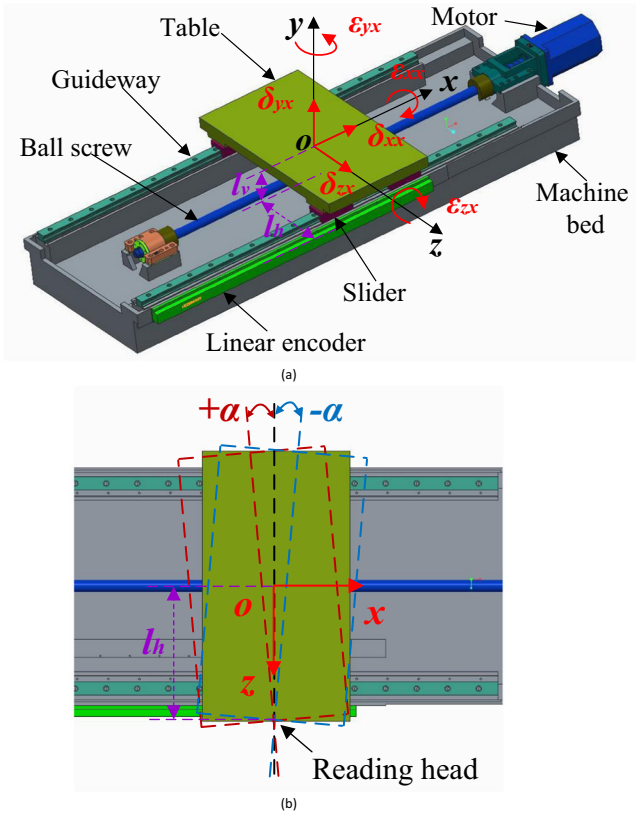

Fig. 1 Repeatability of positioning effected by table motion pose. **a** Six directional errors in translational axis. **b** Different table motion poses in same position

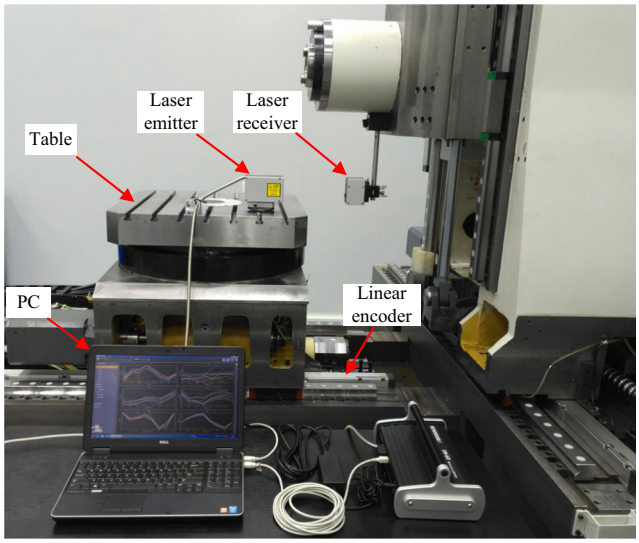

Fig. 2 Motion error measurement

emitter and the linear encoder are in a plane in the vertical direction. The experiment was performed five times, and the results are averaged as shown in Fig. 3. It can be seen that the image of positional deviation $X_{i,\,j}$ is similar to the pitch angleε_{zx}. This is because the laser interferometer and the linear encoder are in a plane in the vertical direction; the Abbe error in the vertical direction has great influence on the positional deviation, while the Abbe error in the horizontal direction has less influence. Similarly, if the laser interferometer and the linear encoder are placed in a plane in the horizontal direction, the Abbe error in the horizontal direction has a great influence on the positional deviation. This indicates that the pitch angle (ε_{zx}) and yaw angle (ε_{yx}) are important factors that influence the positional deviation of the linear motion table.

The mechanism of repeatability of positioning based on motion pose of table is proposed. In further detail, the table moves to a position n times, and there are n motion pose types (^1T_i, ^2T_i, …, ^nT_i). The motion poses are different ($^1T_i \neq {}^2T_i \neq \ldots \neq {}^nT_i$), leading to a variation in the positional deviation ($X_{i,\,1} \neq X_{i,\,2} \neq \ldots \neq X_{i,\,n}$), which describes the mechanism of repeatability of positioning. Using a yaw angle example, the table moves into a position twice, their motion poses are different (the yaw angles are $+\alpha$ and $-\alpha$, respectively) and will lead to the positional deviation that is different, as shown in Fig. 1b.

Because ${}^j\delta_{zx,\,i}$, ${}^j\varepsilon_{yx,\,i}$ and ${}^j\delta_{yx,\,i}$, ${}^j\varepsilon_{zx,\,i}$ are small second-order quantities that can be neglected, Eq. (5) can be simplified as

$$X_{i,j} = l_h{}^j\varepsilon_{yx,i} + l_v{}^j\varepsilon_{zx,i} + e_{L,i} \tag{6}$$

$\varepsilon_{yx,\,i}$ and $\varepsilon_{zx,\,i}$ are two separate angles; the variance of both sides of Eq. (6) is taken, the following equation can be obtained:

$$S_i^2 = l_h^2 S_{\varepsilon_{yx,i}}^2 + l_v^2 S_{\varepsilon_{zx,i}}^2 \tag{7}$$

It can be seen that S_i is affected by $S_{\varepsilon_{yx,i}}$ and $S_{\varepsilon_{zx,i}}$, which means that the repeatability of positioning is affected by the motion pose (yaw and pitch angle) of the table. Therefore, it is necessary to analyze the motion pose during the table movement process, which is mainly affected by geometrical errors.

3 Theoretical analysis

3.1 Analysis of pitch and yaw angle affected by geometrical errors

It is assumed that the guideway and table are rigid, and the deformation is from the slider component, which contains a slider and steel ball [22]. The table moves in the x-direction, the geometric errors of guideways in both the z- and y-directions, which can be expressed as e_{h1}, e_{h2}, e_{v1}, and e_{v2}, respectively, as shown in Fig. 4 and Fig. 5. The table moves along the guideway through the four sliders. Assuming that the table moves from x_{i-m} to x_{i+m}, the force scheme of the system is shown in Fig. 4. Where l_1 is the distance between the two

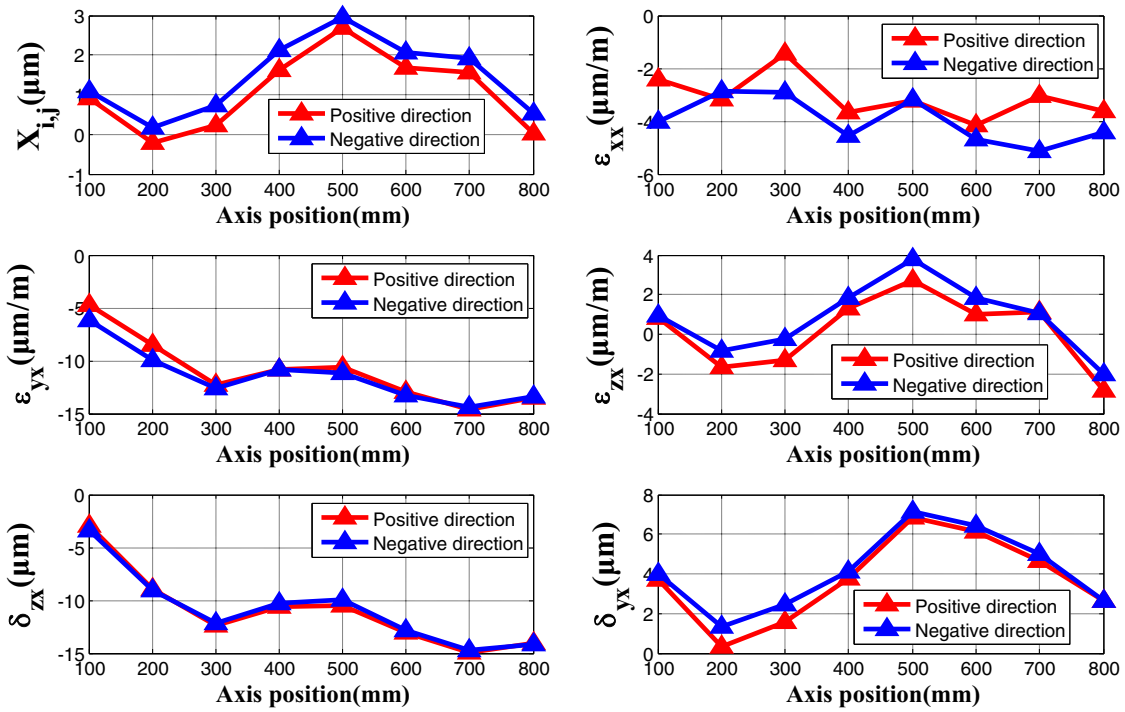

Fig. 3 Measurement results of motion errors

sliders in the same guideway, l_2 is the distance between two guideways; $P_{h1,\,i}$, $P_{h2,\,i}$, $P_{h3,\,i}$, and $P_{h4,\,i}$ are the reaction forces between the sliders and guideways in the z-direction (horizontal direction) at x_i; $P_{v1,\,i}$, $P_{v2,\,i}$, $P_{v3,\,i}$, and $P_{v4,\,i}$ are the reaction

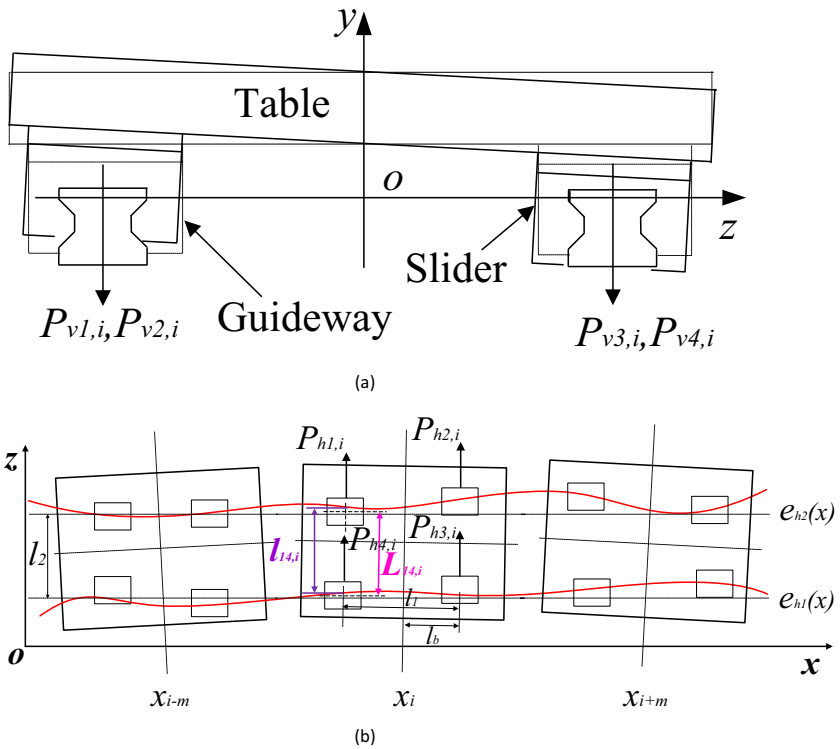

Fig. 4 Force scheme of guideway-slider subsystem in actual conditions. **a** Force diagram of y-directions. **b** Force diagram of z-directions

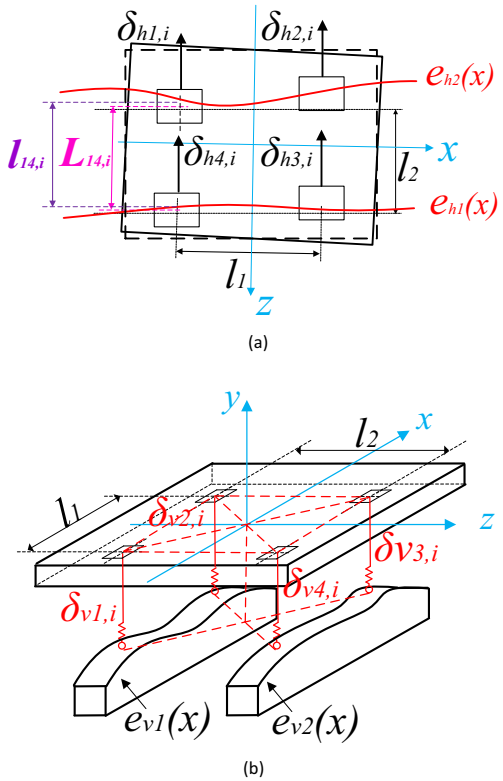

Fig. 5 Deformation of guideway-slider subsystem. **a** z-direction displacement. **b** y-direction displacement

forces between the sliders and guideways in the y-direction (vertical direction) .

The force equilibrium equation at x_i can be expressed as

$$\begin{cases} P_{h1,i}+P_{h2,i}+P_{h3,i}+P_{h4,i}=0 \\ \frac{l_1}{2}\left(P_{h1,i}-P_{h2,i}-P_{h3,i}+P_{h4,i}\right)=0 \\ P_{v1,i}+P_{v2,i}+P_{v3,i}+P_{v4,i}=0 \\ \frac{l_2}{2}\left(P_{v1,i}+P_{v2,i}-P_{v3,i}-P_{v4,i}\right)+M_x=0 \\ \frac{l_1}{2}\left(-P_{v1,i}+P_{v2,i}+P_{v3,i}-P_{v4,i}\right)=0 \end{cases} \tag{8}$$

where is the x-direction moment that acting on the table.

The deformation of the guideway-slider subsystem is effected by geometrical errors as shown in Fig. 5. Since the table is rigid, the deformation compatibility equation can be obtained as follows:

$$\begin{cases} \delta_{h1,i}=\delta_{h4,i}+\delta_{h14,i} \\ \delta_{h2,i}=\delta_{h3,i}+\delta_{h23,i} \\ \delta_{v1,i}+\delta_{v3,i}+\delta_{v13,i}=\delta_{v2,i}+\delta_{v4,i}+\delta_{v24,i} \end{cases} \tag{9}$$

where

$$\begin{cases} \delta_{h14,i} = l_{14,i}-L_{14,i}=e_{h2}(x_{i-l_b})-e_{h1}(x_{i-l_b})\ -L_{14,i} \\ \delta_{h23,i} = l_{23,i}-L_{23,i}=e_{h2}(x_{i+l_b})-e_{h1}(x_{i+l_b})-L_{23,i} \\ \delta_{v13,i}=h_{13,i}-H_{13,i}=e_{v1}(x_{i-l_b})-e_{v2}(x_{i+l_b})-H_{13,i} \\ \delta_{v24,i}=h_{24,i}-H_{24,i}=e_{v1}(x_{i+l_b})-e_{v2}(x_{i-l_b})-H_{24,i} \\ \delta_{hj,i}=\frac{P_{hj,i}}{K_{Sh}}, j=1,2,3,4 \\ \delta_{vj,i}=\frac{P_{vj,i}}{K_{Sv}}, j=1,2,3,4 \end{cases} \tag{10}$$

In the above, $L_{14,\,i}$ denotes the distance between sliders 1 and 4 in the z-direction; $L_{23,\,i}$ indicates the distance between sliders 2 and 3 in the z-direction; $l_{14,\,i}$is the distance between two guideways at the position of slider 1 (or 4) in the z-direction; and $l_{23,\,i}$denotes the distance between two guideways at the position of slider 2(or 3) in the$z$-direction; in addition, $\delta_{h14,\,i}$ denotes the difference between $l_{14,\,i}$ and $L_{14,\,i}$; $\delta_{h23,\,i}$ is the difference between $l_{23,\,i}$ and $L_{23,\,i}$; $H_{13,\,i}$ indicates the distance between sliders 1 and 3 in the y-direction, $H_{24,\,i}$ is the distance between sliders 2 and 4 in the$y$-direction, $h_{13,\,i}$ indicates the geometric error between two guideways at the position of sliders 1 and 3 in the y-direction, and $h_{24,\,i}$ indicates the geometric error between two guideways at the position of sliders 2 and 4 in the y-direction. Finally, $\delta_{v13,\,i}$ denotes the difference between $h_{13,\,i}$ and $H_{13,\,i}$; $\delta_{v24,\,i}$ is the difference between $h_{24,\,i}$and $H_{24,\,i}$. K_{Sh} and K_{Sv} indicate the stiffness of the slider component in the z- and y-directions, respectively.

According to Eq. (8) and Eq. (9), when the table moves to x_i in the kth time in the positive direction, the yaw and pitch angles of the table can be expressed as follows:

$$\begin{cases} {}^k\varepsilon_{yx,i}\uparrow \approx \tan{}^k\varepsilon_{yx,i}\uparrow = \dfrac{{}^k\delta_{1h,i}\uparrow - {}^k\delta_{2h,i}\uparrow}{l_1} = \dfrac{{}^k\delta_{h14,i}\uparrow}{2l_1} - \dfrac{{}^k\delta_{h23,i}\uparrow}{2l_1} \\ {}^k\varepsilon_{zx,i}\uparrow \approx \tan{}^k\varepsilon_{zx,i}\uparrow = \dfrac{{}^k\delta_{1v,i}\uparrow - {}^k\delta_{2v,i}\uparrow}{l_1} = \dfrac{{}^k\delta_{v24,i}\uparrow}{2l_1} - \dfrac{{}^k\delta_{v13,i}\uparrow}{2l_1} \end{cases} \tag{11}$$

If the elastic deformation $\delta_{hj,\,i}$ and $\delta_{vj,\,i}$ are not fully recovered, it will affect the motion pose of table atx_{i+1}. In order to study the recovery of the elastic deformation of the slider component, an experiment was carried out as shown in Fig. 6. A cylinder and lifting system were used to apply the load on the side of slider. A force sensor, which is installed on the end of the cylinder, was used for collecting force signals. An eddy current sensor was used to measure the displacements of the slider. The force was increased from 0 N to a certain value, the displacement of the slider was measured; then, the force was reduced to 0 N and the displacement was measured again. If the two measurements are different, the elastic deformation of the slider is not fully recovered. The change of force is 0 N → 1000 N → 0 N →

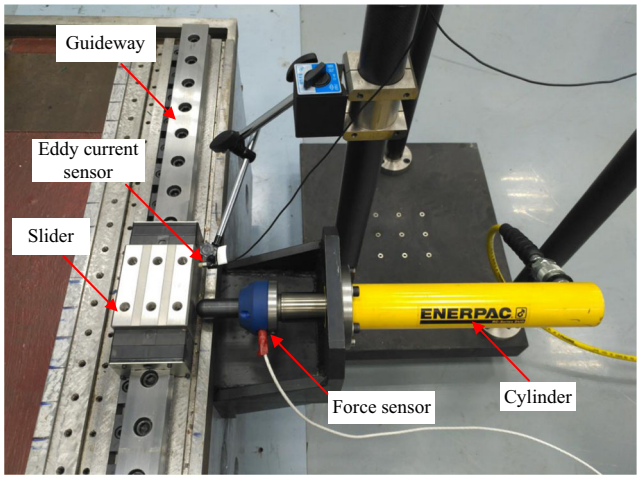

Fig. 6 Experimental setup for the force-displacement measure

$$
\begin{aligned}
{}^{k}L_{14,i+1}\uparrow &= {}^{k}L_{14,i}\uparrow + {}^{k}\Delta_{h14,i}\uparrow \\
&= {}^{k}L_{14,i}\uparrow + \frac{{}^{k}P_{h1,i}\uparrow}{K_{Sh}}{}^{k}q_{h1,i}\uparrow + \frac{{}^{k}P_{h4,i}\uparrow}{K_{Sh}}{}^{k}q_{h4,i}\uparrow \qquad (12)\\
{}^{k}L_{23,i+1}\uparrow &= {}^{k}L_{23,i}\uparrow + {}^{k}\Delta_{h23,i}\uparrow \\
&= {}^{k}L_{23,i}\uparrow + \frac{{}^{k}P_{h2,i}\uparrow}{K_{Sh}}{}^{k}q_{h2,i}\uparrow + \frac{{}^{k}P_{h3,i}\uparrow}{K_{Sh}}{}^{k}q_{h3,i}\uparrow \qquad (13)\\
{}^{k}H_{13,i+1}\uparrow &= {}^{k}H_{13,i}\uparrow + {}^{k}\Delta_{v13,i}\uparrow \\
&= {}^{k}H_{13,i}\uparrow + \frac{{}^{k}P_{v1,i}\uparrow}{K_{Sv}}{}^{k}q_{v1,i}\uparrow + \frac{{}^{k}P_{v3,i}\uparrow}{K_{Sv}}{}^{k}q_{v3,i}\uparrow \qquad (14)\\
{}^{k}H_{24,i+1}\uparrow &= {}^{k}H_{24,i}\uparrow + {}^{k}\Delta_{v24,i}\uparrow \\
&= {}^{k}H_{24,i}\uparrow + \frac{{}^{k}P_{v2,i}\uparrow}{K_{Sv}}{}^{k}q_{v2,i}\uparrow + \frac{{}^{k}P_{v4,i}\uparrow}{K_{Sv}}{}^{k}q_{v4,i}\uparrow \qquad (15)
\end{aligned}
$$

2000 N → 0 N → 3000 N → 0 N → 4000 N → 0 N → 5000 N → 0 N → 6000 N → 0 N → 7000 N → 0 N in the experiment process. The experiments were carried out five times, and results were averaged as shown in Fig. 7. The red line represents the displacement after exerting a force, and the green for removing the force. It can be seen that the displacement of the slider increases with the increase of force, and the displacement of the slider does not return to the initial value after removing the force. The no-recovered elastic deformations are 53.5, 24, 29.1, 24.3, 23.4, 17.7, and 17.2%, respectively. It indicates that the elastic deformation caused by geometric errors are not fully recovered; it will affect the motion pose of table in the next position.

When the table moves to x_{i+1} in kth time in the positive direction, the distances between the slider components in the horizontal and vertical directions will change as a result of no-recovered elastic deformation, which can be expressed as follows.

where ${}^{k+}\Delta_{hjk,\,i}$ (or ${}^{k+}\Delta_{vjk,\,i}$) denotes the no-recovered elastic deformation of sliders j and k owing to geometrical errors of the guideways at x_i in the horizontal (or vertical) direction; $q_{hj,\,i}$ and $q_{vj,\,i}$ denote no-recovery ratio of slider j component elastic deformation at x_i in the horizontal and vertical direction.

The yaw and pitch angles of the table can be obtained as follows:

$$
\begin{cases}
{}^{k}\varepsilon_{yx,i+1}\uparrow \approx \tan{}^{k}\varepsilon_{yx,i+1}\uparrow = \dfrac{{}^{k}\delta_{1h,i+1}\uparrow - {}^{k}\delta_{2h,i+1}\uparrow}{l_1} \\
\qquad = \dfrac{{}^{k}\delta_{h14,i+1}\uparrow}{2l_1} - \dfrac{{}^{k}\delta_{h23,i+1}\uparrow}{2l_1} \\
{}^{k}\varepsilon_{zx,i+1}\uparrow \approx \tan{}^{k}\varepsilon_{zx,i+1}\uparrow = \dfrac{{}^{k}\delta_{1v,i+1}\uparrow - {}^{k}\delta_{2v,i+1}\uparrow}{l_1} \\
\qquad = \dfrac{{}^{k}\delta_{v24,i+1}\uparrow}{2l_1} - \dfrac{{}^{k}\delta_{v13,i+1}\uparrow}{2l_1}
\end{cases} \qquad (16)
$$

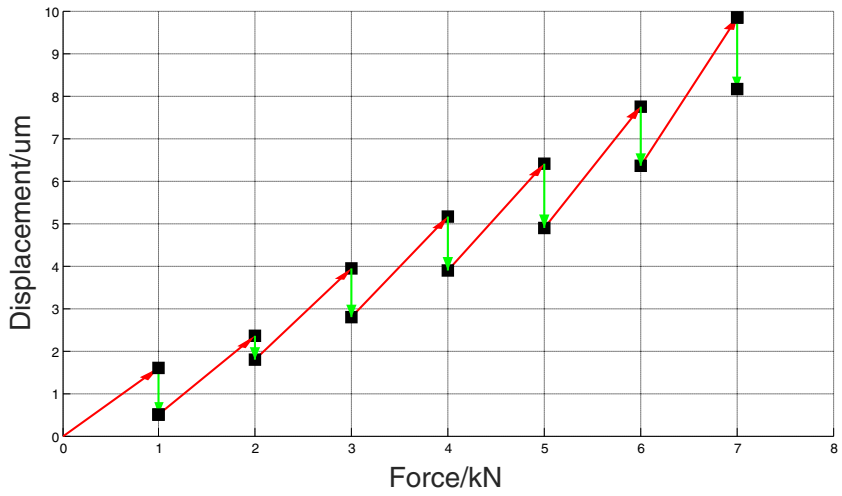

Fig. 7 The curve of force-displacement

where

$$\begin{cases} {}^{k}\delta_{h14,i+1}\uparrow = l_{14,i+1} - {}^{k}L_{14,i+1}\uparrow \\ {}^{k}\delta_{h23,i+1}\uparrow = l_{23,i+1} - {}^{k}L_{23,i+1}\uparrow \\ {}^{k}\delta_{v13,i+1}\uparrow = h_{13,i+1} - {}^{k}H_{13,i+1}\uparrow \\ {}^{k}\delta_{v24,i+1}\uparrow = h_{24,i+1} - {}^{k}H_{24,i+1}\uparrow \end{cases} \tag{17}$$

3.2 Analysis of the table motion pose based on point-by-point recursion

An approach for analyzing the table motion pose on the consideration of the no-recovered elastic deformation based on point-by-point recursion is proposed. In further detail, the no-recovered elastic deformation of the slider components generated at x_i should be drawn into the computational process of the table pose at x_{i+1}. Through this analogy, the table moves back and forth n times along the guideways, the distances of the slider components in the horizontal and vertical directions will change as a result of no-recovered elastic deformation, and can be expressed as follows (the derivation procedure is presented in Appendix A).

$$\begin{aligned} {}^{(k+n)}L_{14,i}\uparrow &= {}^{(k+n)}L_{14,i-1}\uparrow + {}^{(k+n)}\Delta_{h14,i-1}\uparrow \\ &= {}^{k}L_{14,i}\uparrow + \sum_{j=i}^{i+m}\left(\frac{{}^{k}P_{h1,j}\uparrow}{K_{Sh}}{}^{k}q_{h1,j}\uparrow + \frac{{}^{k}P_{h4,j}\uparrow}{K_{Sh}}{}^{k}q_{h4,j}\uparrow\right) \\ &+ \sum_{t=k}^{k+n-1}\sum_{j=i-m+1}^{i+m-1}\left(\frac{{}^{t}P_{h1,j}\downarrow}{K_{Sh}}{}^{t}q_{h1,j}\downarrow + \frac{{}^{t}P_{h4,j}\downarrow}{K_{Sh}}{}^{t}q_{h4,j}\downarrow\right) \\ &+ \sum_{t=k+1}^{k+n-1}\sum_{j=i-m}^{i+m}\left(\frac{{}^{t}P_{h1,j}\uparrow}{K_{Sh}}{}^{t}q_{h1,j}\uparrow + \frac{{}^{t}P_{h4,j}\uparrow}{K_{Sh}}{}^{t}q_{h4,j}\uparrow\right) \\ &+ \sum_{j=i-m}^{i-1}\left(\frac{{}^{(k+n)}P_{h1,j}\uparrow}{K_{Sh}}{}^{(k+n)}q_{h1,j}\uparrow + \frac{{}^{(k+n)}P_{h4,j}\uparrow}{K_{Sh}}{}^{(k+n)}q_{h4,j}\uparrow\right) \end{aligned} \tag{18}$$

$$\begin{aligned} {}^{(k+n)}L_{23,i}\uparrow &= {}^{(k+n)}L_{23,i-1}\uparrow + {}^{(k+n)}\Delta_{h23,i-1}\uparrow \\ &= {}^{k}L_{23,i}\uparrow + \sum_{j=i}^{i+m}\left(\frac{{}^{k}P_{h2,j}\uparrow}{K_{Sh}}{}^{k}q_{h2,j}\uparrow + \frac{{}^{k}P_{h3,j}\uparrow}{K_{Sh}}{}^{k}q_{h3,j}\uparrow\right) \\ &+ \sum_{t=k}^{k+n-1}\sum_{j=i-m+1}^{i+m-1}\left(\frac{{}^{t}P_{h2,j}\downarrow}{K_{Sh}}{}^{t}q_{h2,j}\downarrow + \frac{{}^{t}P_{h3,j}\downarrow}{K_{Sh}}{}^{t}q_{h3,j}\downarrow\right) \\ &+ \sum_{t=k+1}^{k+n-1}\sum_{j=i-m}^{i+m}\left(\frac{{}^{t}P_{h2,j}\uparrow}{K_{Sh}}{}^{t}q_{h2,j}\uparrow + \frac{{}^{t}P_{h3,j}\uparrow}{K_{Sh}}{}^{t}q_{h3,j}\uparrow\right) \\ &+ \sum_{j=i-m}^{i-1}\left(\frac{{}^{(k+n)}P_{h2,j}\uparrow}{K_{Sh}}{}^{(k+n)}q_{h2,j}\uparrow + \frac{{}^{(k+n)}P_{h3,j}\uparrow}{K_{Sh}}{}^{(k+n)}q_{h3,j}\uparrow\right) \end{aligned} \tag{19}$$

$$\begin{aligned} {}^{(k+n)}H_{13,i}\uparrow &= {}^{(k+n)}H_{13,i-1}\uparrow + {}^{(k+n)}\Delta_{v13,i-1}\uparrow \\ &= {}^{k}H_{13,i}\uparrow + \sum_{j=i}^{i+m}\left(\frac{{}^{k}P_{v1,j}\uparrow}{K_{Sv}}{}^{k}q_{v1,j}\uparrow + \frac{{}^{k}P_{v3,j}\uparrow}{K_{Sv}}{}^{k}q_{v3,j}\uparrow\right) \\ &+ \sum_{t=k}^{k+n-1}\sum_{j=i-m+1}^{i+m-1}\left(\frac{{}^{t}P_{v1,j}\downarrow}{K_{Sv}}{}^{t}q_{v1,j}\downarrow + \frac{{}^{t}P_{v3,j}\downarrow}{K_{Sv}}{}^{t}q_{v3,j}\downarrow\right) \\ &+ \sum_{t=k+1}^{k+n-1}\sum_{j=i-m}^{i+m}\left(\frac{{}^{t}P_{v1,j}\uparrow}{K_{Sv}}{}^{t}q_{v1,j}\uparrow + \frac{{}^{t}P_{v3,j}\uparrow}{K_{Sv}}{}^{t}q_{v3,j}\uparrow\right) \\ &+ \sum_{j=i-m}^{i-1}\left(\frac{{}^{(k+n)}P_{v1,j}\uparrow}{K_{Sv}}{}^{(k+n)}q_{v1,j}\uparrow + \frac{{}^{(k+n)}P_{v3,j}\uparrow}{K_{Sv}}{}^{(k+n)}q_{v3,j}\uparrow\right) \end{aligned} \tag{20}$$

$$\begin{aligned} {}^{(k+n)}H_{24,i}\uparrow &= {}^{(k+n)}H_{24,i-1}\uparrow + {}^{(k+n)}\Delta_{v24,i-1}\uparrow \\ &= {}^{k}H_{24,i}\uparrow + \sum_{j=i}^{i+m}\left(\frac{{}^{k}P_{v2,j}\uparrow}{K_{Sv}}{}^{k}q_{v2,j}\uparrow + \frac{{}^{k}P_{v4,j}\uparrow}{K_{Sv}}{}^{k}q_{v4,j}\uparrow\right) \\ &+ \sum_{t=k}^{k+n-1}\sum_{j=i-m+1}^{i+m-1}\left(\frac{{}^{t}P_{v2,j}\downarrow}{K_{Sv}}{}^{t}q_{v2,j}\downarrow + \frac{{}^{t}P_{v4,j}\downarrow}{K_{Sv}}{}^{t}q_{v4,j}\downarrow\right) \\ &+ \sum_{t=k+1}^{k+n-1}\sum_{j=i-m}^{i+m}\left(\frac{{}^{t}P_{v2,j}\uparrow}{K_{Sv}}{}^{t}q_{v2,j}\uparrow + \frac{{}^{t}P_{v4,j}\uparrow}{K_{Sv}}{}^{t}q_{v4,j}\uparrow\right) \\ &+ \sum_{j=i-m}^{i-1}\left(\frac{{}^{(k+n)}P_{v2,j}\uparrow}{K_{Sv}}{}^{(k+n)}q_{v2,j}\uparrow + \frac{{}^{(k+n)}P_{v4,j}\uparrow}{K_{Sv}}{}^{(k+n)}q_{v4,j}\uparrow\right) \end{aligned} \tag{21}$$

The yaw and pitch angles of the table at position x_i in $k+n$th time in the positive direction can be expressed as follows:

$$\begin{cases} {}^{(k+n)}\varepsilon_{yx,i}\uparrow \approx \tan{}^{(k+n)}\varepsilon_{yx,i}\uparrow = \dfrac{{}^{(k+n)}\delta_{1h,i}\uparrow - {}^{(k+n)}\delta_{2h,i}\uparrow}{l_1} \\ \qquad\qquad = \dfrac{{}^{(k+n)}\delta_{h14,i}\uparrow}{2l_1} - \dfrac{{}^{(k+n)}\delta_{h23,i}\uparrow}{2l_1} \\ {}^{(k+n)}\varepsilon_{zx,i}\uparrow \approx \tan{}^{(k+n)}\varepsilon_{zx,i}\uparrow = \dfrac{{}^{(k+n)}\delta_{1v,i}\uparrow - {}^{(k+n)}\delta_{2v,i}\uparrow}{l_1} \\ \qquad\qquad = \dfrac{{}^{(k+n)}\delta_{v24,i}\uparrow}{2l_1} - \dfrac{{}^{(k+n)}\delta_{v13,i}\uparrow}{2l_1} \end{cases} \tag{22}$$

where

$$\begin{cases} {}^{(k+n)}\delta_{h14,i} \uparrow = l_{14,i} - {}^{(k+n)}L_{14,i}\uparrow \\ {}^{(k+n)}\delta_{h23,i} \uparrow = l_{23,i} - {}^{(k+n)}L_{23,i}\uparrow \\ {}^{(k+n)}\delta_{v13,i} \uparrow = h_{13,i} - {}^{(k+n)}H_{13,i}\uparrow \\ {}^{(k+n)}\delta_{v24,i} \uparrow = h_{24,i} - {}^{(k+n)}H_{24,i}\uparrow \end{cases} \tag{23}$$

From the above-mentioned analysis, the $2(n+1)+1$ yaw and pitch angles can be obtained at x_i, and the $2(n+1)$ yaw and pitch angles can be obtained at other positions.

The standard uncertainty of the yaw and pitch angles in the positive and negative directions, respectively, can be obtained and expressed as follows.

$$S_{\varepsilon_{yx,i}\uparrow} = \sqrt{\frac{1}{n-1}\sum_{j=1}^{n}\left(\varepsilon_{yx,i}\uparrow - \overline{\varepsilon}_{yx,i}\uparrow\right)} \tag{24}$$

$$S_{\varepsilon_{yx,i}\downarrow} = \sqrt{\frac{1}{n-1}\sum_{j=1}^{n}\left(\varepsilon_{yx,i}\downarrow - \overline{\varepsilon}_{yx,i}\downarrow\right)} \tag{25}$$

$$S_{\varepsilon_{zx,i}\uparrow} = \sqrt{\frac{1}{n-1}\sum_{j=1}^{n}\left(\varepsilon_{zx,i}\uparrow - \overline{\varepsilon}_{zx,i}\uparrow\right)} \tag{26}$$

$$S_{\varepsilon_{zx,i}\downarrow} = \sqrt{\frac{1}{n-1}\sum_{j=1}^{n}\left(\varepsilon_{zx,i}\downarrow - \overline{\varepsilon}_{zx,i}\downarrow\right)} \tag{27}$$

The bidirectional standard uncertainty of the yaw and pitch angles in a position can be expressed as follows:

$$S_{\varepsilon_{yx,i}} = \max\left[S_{\varepsilon_{yx,i}}\uparrow; S_{\varepsilon_{yx,i}}\downarrow\right] \tag{28}$$

$$S_{\varepsilon_{zx,i}} = \max\left[S_{\varepsilon_{zx,i}}\uparrow; S_{\varepsilon_{zx,i}}\downarrow\right] \tag{29}$$

3.3 Geometric error optimization based on genetic algorithm

It can be seen from Eq. (7) that the minimum $S_{X_{ij}}$ can be achieved, when $S_{\varepsilon_{zx,i}}$ and $S_{\varepsilon_{yx,i}}$ are the minimum values. To determine the optimal values of e_{h2} and e_{v2}, e_{h1} and e_{v1} are taken as reference values, and $min\left(S_{\varepsilon_{yx,i}}\right)$ and $min\left(S_{\varepsilon_{zx,i}}\right)$ are regarded as the target functions, which are expressed by as Eq. (30) and Eq. (31), respectively.

$$\min\begin{Bmatrix} S_{\varepsilon_{yx,i-m}} = f_{i-m}(e_{h2}(x_{i-m}),\ldots,e_{h2}(x_i),\ldots,e_{h2}(x_{i+m})), \\ \cdots \\ S_{\varepsilon_{yx,i}} = f_i(e_{h2}(x_{i-m}),\ldots,e_{h2}(x_i),\ldots,e_{h2}(x_{i+m})), \\ \cdots \\ S_{\varepsilon_{yx,i+m}} = f_{i+m}(e_{h2}(x_{i-m}),\ldots,e_{h2}(x_i),\ldots,e_{h2}(x_{i+m})) \end{Bmatrix} \tag{30}$$

$$\min\begin{Bmatrix} S_{\varepsilon_{zx,i-m}} = g_{i-m}(e_{v2}(x_{i-m}),\ldots,e_{v2}(x_i),\ldots,e_{v2}(x_{i+m})), \\ \cdots \\ S_{\varepsilon_{zx,i}} = g_i(e_{v2}(x_{i-m}),\ldots,e_{v2}(x_i),\ldots,e_{v2}(x_{i+m})), \\ \cdots \\ S_{\varepsilon_{zx,i+m}} = g_{i+m}(e_{v2}(x_{i-m}),\ldots,e_{v2}(x_i),\ldots,e_{v2}(x_{i+m})) \end{Bmatrix} \tag{31}$$

4 Results of theoretical calculation

During the process of the guideway error optimization, e_{h1} and e_{v1} are set to arbitrary values, $q_{hj,\,i}$ and $q_{vj,\,i}$ are set up as a constant. The optimal results are $e_{h2}(x_i) = e_{h1}(x_i) + l_2$ and $e_{v2}(x_i) = e_{v1}(x_i)$, as shown in Fig. 8. The standard uncertainties of the yaw and pitch angles will reach the minimum if the errors of the two guideways are the same in horizontal and vertical direction. This can be attributed to the fact that $\delta_{h14,\,i} = \delta_{h23,\,i} = 0$ and $\delta_{v24,\,i} = \delta_{v13,\,i}$, which agrees with Eq. (11).

To study the influence of the guideway error amplitude on the table motion pose, the following process is carried out. Assuming that e_{h1} and e_{h2} have sinusoidal geometrical errors with amplitudes A_{h1} andA_{h2}, respectively, keeping A_{h1} unchanged and changing the ration of $(A_{h2} - A_{h1})/A_{h1}$ from − 1 to 1, the step length is 0.2, as shown in Fig. 9, and the standard uncertainty of the yaw angle at different ratios is calculated. Figure 10a shows the results; it can be seen that the standard uncertainty of the yaw angle decreases with the $(A_{h2} - A_{h1})/A_{h1}$ ration being changed from − 1 to 0 and increases with the ration being changed from 0 to 1, whereas the standard uncertainty of the yaw angle reaches the minimum when the ration is zero. At this point, the amplitudes of the two guideways are the same, that is, $A_{h1} = A_{h2}$. This indicates that closer error amplitudes of the two guideways will result in less standard uncertainty of the yaw angle. Similarly, the error in the vertical direction as illustrated in Fig. 10b.

5 Experiment validation

Experiments were carried out on a linear motion test table in a constant temperature environment of 20 ± 0.5 °C. As shown in Fig. 11, the table is driven by a*FANUC* α *iS* motor and controlled by a *FANUC* 0*i F* numerical control system. The specifications of the table are listed in Table 1. A laser interferometer (Renishaw XL80) is used to measure the pitch and yaw.

The experiment was carried out in two steps. First, the geometric errors of the guideways in the vertical direction

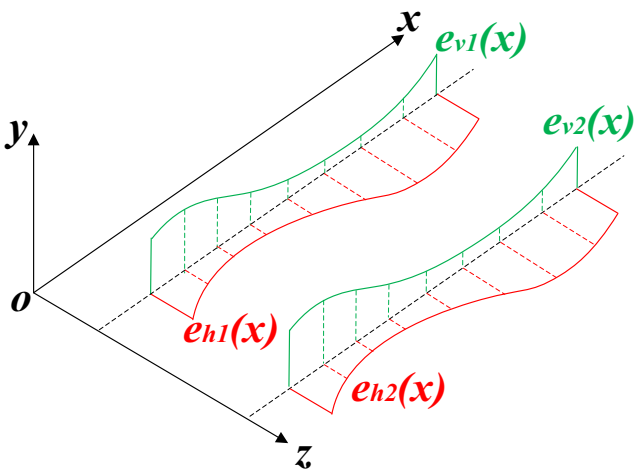

Fig. 8 Optimization results

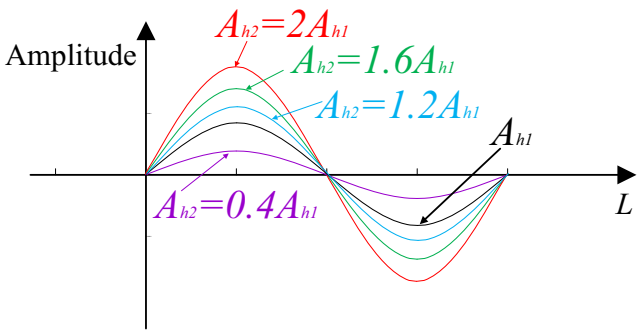

Fig. 9 Different error amplitudes of guideways

were adjusted, and the pitch angles under different error forms were measured. Second, the geometric errors of the guideways in the horizontal direction were adjusted, and the yaw angle and positioning error under different error situations were tested.

The geometric errors of guideway 1 in the vertical direction e_{v1} was taken as the reference error and measured using a laser interferometer as shown in Fig. 12; the result is shown in Fig. 14a, the minimum of e_{v1} is − 14.8 μm.

The parallelism between the guide 1 and the guide 2 in the vertical direction can be expressed by p_v, and the e_{v2} is the sum of the straightness error of guide 2 and the parallelism p_v. In order to easily adjust e_{v2}, a leveling ruler was placed on the

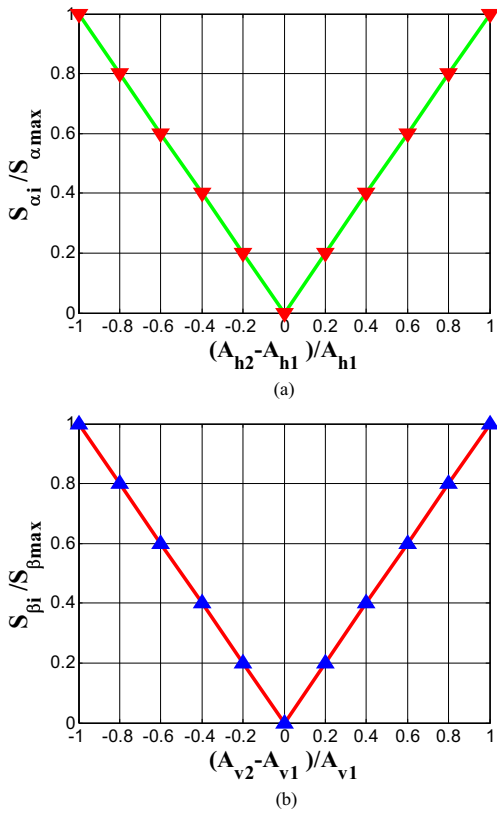

Fig. 10 Variation of angle uncertainty along with error amplitude of guideways. **a** Variation of $S_{\varepsilon_{yx,i}}$ along with A_{h2}. **b** Variation of $S_{\varepsilon_{zx,i}}$ angle along with A_{v2}

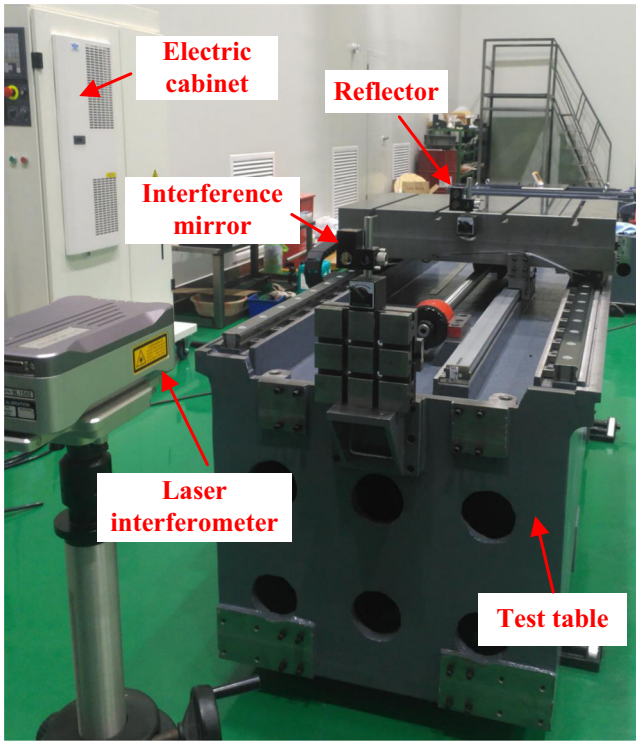

Fig. 11 Linear motion test table used in the experiments

two sliders of guideways, and an electro-level was placed on the leveling ruler, as shown in Fig. 13a. Two sliders were moved simultaneously, and the differences of each position were measured, e_{v2} was changed by scraping the mounting datum according to the measurement as shown in Fig. 13b. Then, the table was installed on the four sliders and moved back and forth five times along guideways. The pitch angles at the midpoint of a stroke were tested using a laser interferometer; ten test datasets were obtained, and the standard uncertainty was calculated.

The experiment was conducted five times, and the result of adjusting the geometric errors of guideway 2 in the vertical direction, e_{v2}, is shown in Fig. 14a, where the $\min(e_{v2}) - \min(e_{v1})$ are − 9.2, − 2.95, 3.16, 5.9, and 8.8 μm, respectively. The pitch angles in each error form were measured and their standard uncertainty were calculated, as shown in Fig. 14b. It can be seen that the standard uncertainty of the pitch angle is reduced from 10.8 to 5.15 μm/m with the change of $\min(e_{v2}) - \min(e_{v1})$ from − 9.2 to − 2.95 μm and increased from 5.6 to 9.7 μm/m with the differences changes from 3.16 to 8.8 μm. It

Table 1 Specifications of the test table

Stroke of motion table	2250 mm
Number of sliders per guideway	2
Length of slider	180 mm
Distance between sliders	400 mm
Distance between two guideways	650 mm

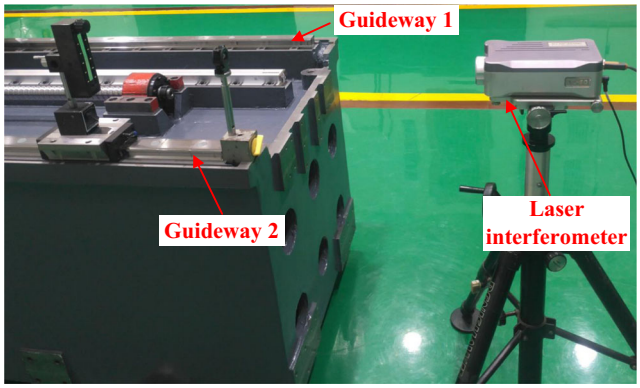

Fig. 12 Guideway geometric error measurement

is indicated that the standard uncertainty of the pitch angle is affected by geometric error of the two guideways in vertical direction; closer error of the two guideways results in smaller standard uncertainty of the pitch angle, which agrees well with the theoretical analysis.

In the second step experiment, the effect of the geometric error in horizontal direction of the guideway on the yaw angle was experimentally validated in the similar way. The geometric error of guideway 2 in the horizontal direction was adjusted by using wedge plate, as shown in Fig. 15b. In order to easily adjust e_{h2}, a dial gauge was installed on the slider of guideway

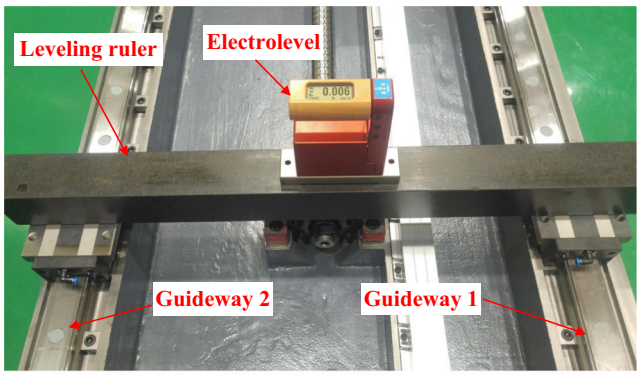

(a)

(b)

Fig. 13 Geometric error adjustment in vertical direction. **a** Error measurement. **b** Error adjustment

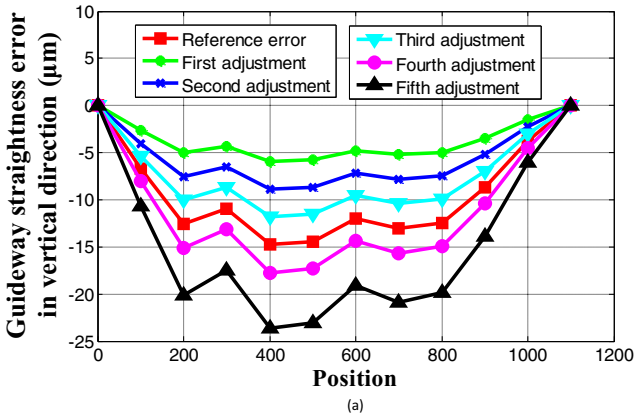

(a)

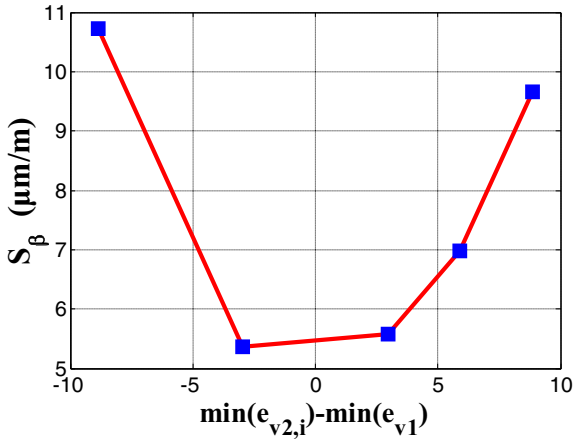

(b)

Fig. 14 Experimental results. **a** Geometrical error of guideways in vertical direction. **b** Variation of standard uncertainty of pitch angle with e_{v2}

2, and the pointer was in contact with the side surface of the slider of guideway 1 as shown in Fig. 15a. Two sliders were moved simultaneously, and the difference of each position was measured. The yaw angles at midpoint of stroke were tested and the standard uncertainty was calculated, as shown in Fig. 16a, b.

It can be seen that the standard uncertainty of the yaw angle is reduced from 1.96 to 0.9 μm/m with the change of $\min(e_{h2}) - \min(e_{h1})$ from − 1.85 to − 0.88 μm and increased from 0.7 to 2.5 μm/m with the difference changes from 0.64 to 2.4 μm. It indicates that the standard uncertainty of the pitch angle is affected by geometric error of the two guideways in horizontal direction, the closer error amplitudes of the two guideways result in smaller standard uncertainty of the yaw angle, which agrees well with the theoretical analysis.

The positional deviations of the table at midpoint of a stroke were tested and the standard uncertainties were calculated in the second step experiment, as shown in Fig. 16c. It can be clearly seen that the standard uncertainty of the positional deviation reduced with a decrease of $\min(e_{h2}) - \min(e_{h1})$, increased with an increase in this difference. This change trend is similar to the pitch angle, which is shown in Fig. 14b.

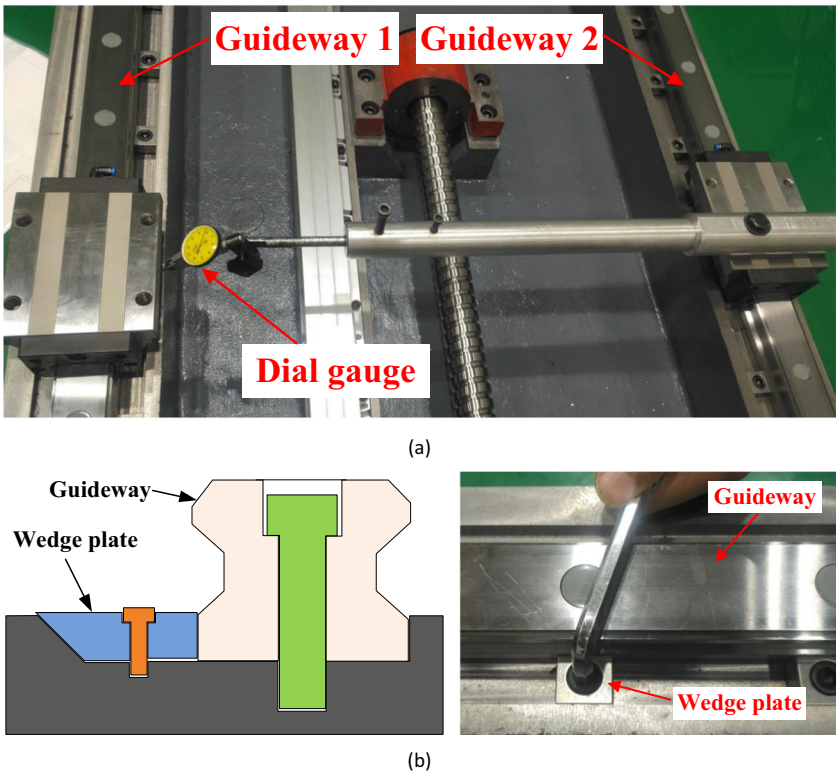

Fig. 15 Geometrical error adjustment and measurement in horizontal direction. **a** Error measurement. **b** Error adjustment

This is because the Abbe arm length of the pitch angle is longer than the yaw angle ($l_v > l_h$), which leads to the pitch angle predominant.

The experimental results indicate that geometrical errors of guideways have an important influence on the repeatability of positioning. And the geometrical errors of guideways are determined by the assembly method. Thus, an assembly method for improving the repeatability of positioning is proposed as shown in Fig. 17.

(1) The assembly of machine tools should be carried out in a constant temperature room of 20 ± 0.5 °C.
(2) Guideway 1 is put on the mounting datum. A torque wrench is used to tighten the fixed screws from the middle to both ends under the same torque, and the geometric error of guideway 1 in the vertical direction (e_{v1}) is measured. If it does not meet the design requirements, the geometrical error is adjusted by scraping the mounting datum.
(3) The geometrical error of guideway 1 in the horizontal directions is changed by adjusting the wedge plate to meet the design requirements.
(4) Guideway 2 is installed on the mounting datum through fixed screws by using a torque wrench, and an electro-level and a leveling ruler are used to measuring the relative error in the vertical directions as shown in Fig. 13a. e_{v2} is changed by scraping the mounting datum according to the measurement to make it approach to e_{v1} as far as possible.
(5) A dial gauge is used to measuring the relative error in the horizontal directions as shown in Fig. 15. e_{h2} is changed by adjusting the wedge plate according to the measurement to make it approach to e_{h1} as far as possible. With those tasks complete, the follow-up work can be carried out.

6 Conclusions

This paper described the effects of geometrical errors of guideways on the repeatability of positioning of linear axes. In addition, the mechanism of repeatability of positioning of linear axes based on the table motion pose was proposed, as was a theoretical model of the geometric errors on the table motion pose based on point-by-point recursion. The assembly method for improving the repeatability of positioning was also proposed. And the following conclusions were drawn:

(1) The mechanism of repeatability of positioning is due to the table motion poses differing during the process of the table moving to a position several times. The repeatability of positioning is affected by the table motion pose; smaller differences between motion poses result in improved repeatability of positioning.
(2) The theoretical model based on point-by-point recursion is a systematic approach for analyzing the table motion pose, which considers the geometrical errors of the guideways. The correctness of this model was verified by experiments. The results indicate that closer

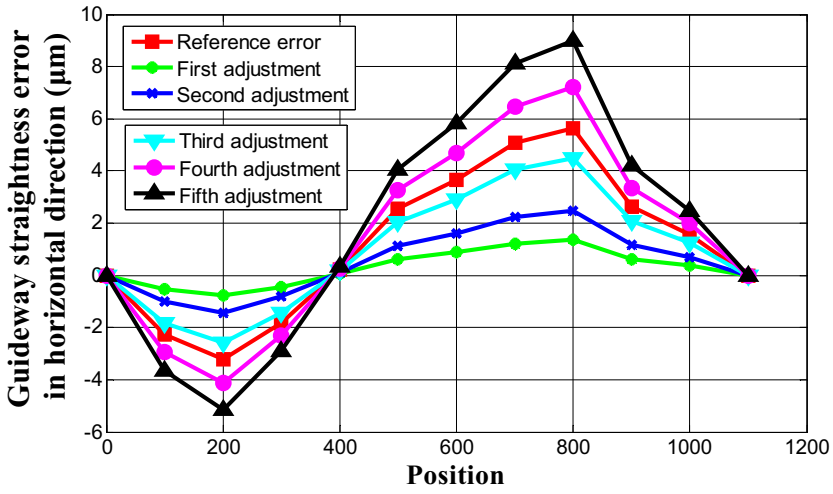

(a)

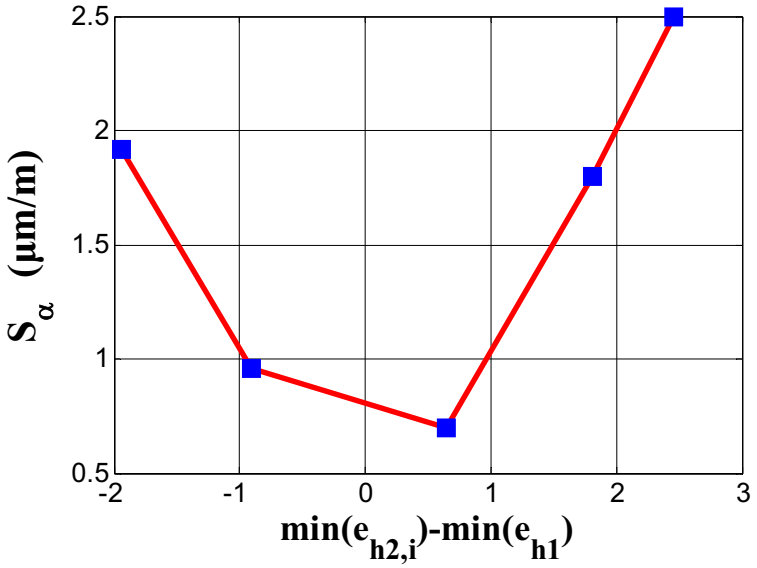

(b)

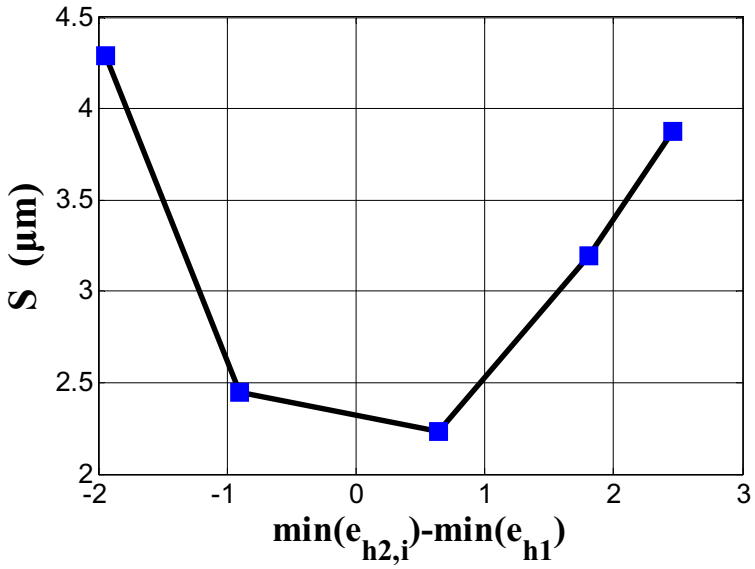

(c)

Fig. 16 Experimental results. **a** Geometrical error of guideways in horizontal direction. **b** Variation of standard uncertainty of yaw angle with e_{h2}. **c** Variation of positional deviation with e_{h2}

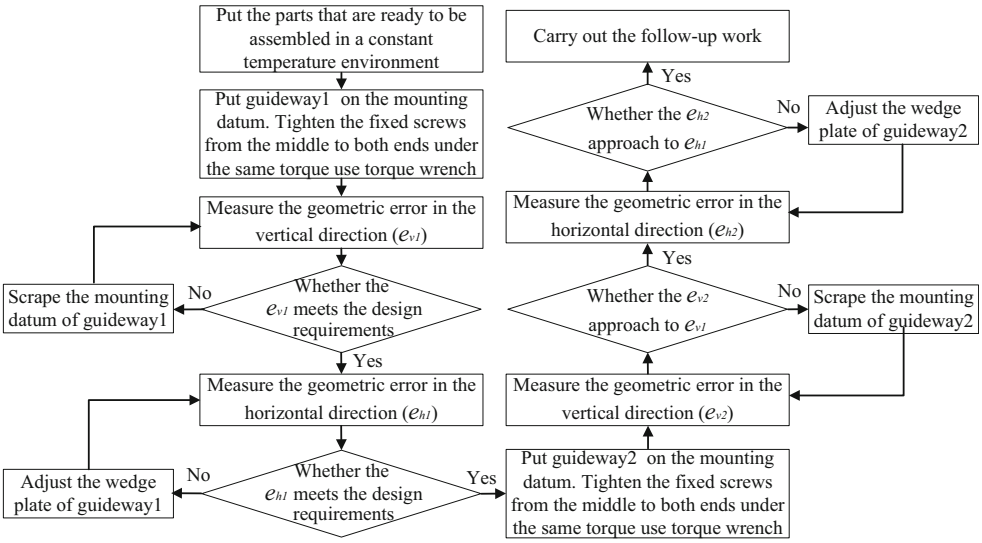

Fig. 17 The assembly method for improving the repeatability of positioning

geometric errors of the two guideways result in better repeatability of positioning.

(3) An assembly method for improving the repeatability of positioning was proposed and verified by the experiments. The merit of this method is that it can provide designers with an informative guideline for improving repeatability of positioning.

Acknowledgements The research is supported by the National Natural Science Foundation of China (No. 51675378) .

Appendix A

$$
\begin{aligned}
{}^{(k+n)}L_{14,i}\uparrow &= {}^{(k+n)}L_{14,i-1}\uparrow + {}^{(k+n)}\Delta_{h14,i-1}\uparrow \\
&= {}^{k}L_{14,i}\uparrow + \sum_{j=i}^{i+m}\left(\frac{{}^{k}P_{h1,j}\uparrow}{K_{Sh}}{}^{k}q_{h1,j}\uparrow + \frac{{}^{k}P_{h4,j}\uparrow}{K_{Sh}}{}^{k}q_{h4,j}\uparrow\right) \\
&\quad + \sum_{j=i-m+1}^{i+m-1}\left(\frac{{}^{k}P_{h1,j}\downarrow}{K_{Sh}}{}^{k}q_{h1,j}\downarrow + \frac{{}^{k}P_{h4,j}\downarrow}{K_{Sh}}{}^{k}q_{h4,j}\downarrow\right) \\
&\quad + \sum_{j=i-m}^{i+m}\left(\frac{{}^{(k+1)}P_{h1,j}\uparrow}{K_{Sh}}{}^{(k+1)}q_{h1,j}\uparrow + \frac{{}^{(k+1)}P_{h4,j}\uparrow}{K_{Sh}}{}^{(k+1)}q_{h4,j}\uparrow\right) \\
&\quad + \sum_{j=i-m+1}^{i+m-1}\left(\frac{{}^{(k+1)}P_{h1,j}\downarrow}{K_{Sh}}{}^{(k+1)}q_{h1,j}\downarrow + \frac{{}^{(k+1)}P_{h4,j}\downarrow}{K_{Sh}}{}^{(k+1)}q_{h4,j}\downarrow\right) + \cdots \qquad \text{(A.1)} \\
&= {}^{k}L_{14,i}\uparrow + \sum_{j=i}^{i+m}\left(\frac{{}^{k}P_{h1,j}\uparrow}{K_{Sh}}{}^{k}q_{h1,j}\uparrow + \frac{{}^{k}P_{h4,j}\uparrow}{K_{Sh}}{}^{k}q_{h4,j}\uparrow\right) \\
&\quad + \sum_{j=i-m}^{i+m}\left(\frac{{}^{(k+n-1)}P_{h1,j}\uparrow}{K_{Sh}}{}^{(k+n-1)}q_{h1,j}\uparrow + \frac{{}^{(k+n-1)}P_{h4,j}\uparrow}{K_{Sh}}{}^{(k+n-1)}q_{h4,j}\uparrow\right) \\
&\quad + \sum_{j=i-m+1}^{i+m-1}\left(\frac{{}^{(k+n-1)}P_{h1,j}\downarrow}{K_{Sh}}{}^{(k+n-1)}q_{h1,j}\downarrow + \frac{{}^{(k+n-1)}P_{h4,j}\downarrow}{K_{Sh}}{}^{(k+n-1)}q_{h4,j}\downarrow\right) \\
&\quad + \sum_{j=i-m}^{i-1}\left(\frac{{}^{(k+n)}P_{h1,j}\uparrow}{K_{Sh}}{}^{(k+n)}q_{h1,j}\uparrow + \frac{{}^{(k+n)}P_{h4,j}\uparrow}{K_{Sh}}{}^{(k+n)}q_{h4,j}\uparrow\right)
\end{aligned}
$$

$$
\begin{aligned}
{}^{(k+n)}L_{23,i}\uparrow &= {}^{(k+n)}L_{23,i-1}\uparrow + {}^{(k+n)}\Delta_{h23,i-1}\uparrow \\
&= {}^{k}L_{23,i}\uparrow + \sum_{j=i}^{i+m}\left(\frac{{}^{k}P_{h2,j}\uparrow}{K_{Sh}}{}^{k}q_{h1,j}\uparrow + \frac{{}^{k}P_{h3,j}\uparrow}{K_{Sh}}{}^{k}q_{h4,j}\uparrow\right) \\
&\quad + \sum_{j=i-m+1}^{i+m-1}\left(\frac{{}^{k}P_{h2,j}\downarrow}{K_{Sh}}{}^{k}q_{h1,j}\downarrow + \frac{{}^{k}P_{h3,j}\downarrow}{K_{Sh}}{}^{k}q_{h4,j}\downarrow\right) \\
&\quad + \sum_{j=i-m}^{i+m}\left(\frac{{}^{(k+1)}P_{h2,j}\uparrow}{K_{Sh}}{}^{(k+1)}q_{h1,j}\uparrow + \frac{{}^{(k+1)}P_{h3,j}\uparrow}{K_{Sh}}{}^{(k+1)}q_{h4,j}\uparrow\right) \\
&\quad + \sum_{j=i-m+1}^{i+m-1}\left(\frac{{}^{(k+1)}P_{h2,j}\downarrow}{K_{Sh}}{}^{(k+1)}q_{h1,j}\downarrow + \frac{{}^{(k+1)}P_{h3,j}\downarrow}{K_{Sh}}{}^{(k+1)}q_{h4,j}\downarrow\right) + \cdots \\
&\quad + \sum_{j=i-m}^{i+m}\left(\frac{{}^{(k+n-1)}P_{h2,j}\uparrow}{K_{Sh}}{}^{(k+n-1)}q_{h1,j}\uparrow + \frac{{}^{(k+n-1)}P_{h3,j}\uparrow}{K_{Sh}}{}^{(k+n-1)}q_{h4,j}\uparrow\right) \\
&\quad + \sum_{j=i-m+1}^{i+m-1}\left(\frac{{}^{(k+n-1)}P_{h2,j}\downarrow}{K_{Sh}}{}^{(k+n-1)}q_{h1,j}\downarrow + \frac{{}^{(k+n-1)}P_{h3,j}\downarrow}{K_{Sh}}{}^{(k+n-1)}q_{h4,j}\downarrow\right) \qquad \text{(A.2)} \\
&\quad + \sum_{j=i-m}^{i-1}\left(\frac{{}^{(k+n)}P_{h2,j}\uparrow}{K_{Sh}}{}^{(k+n)}q_{h1,j}\uparrow + \frac{{}^{(k+n)}P_{h3,j}\uparrow}{K_{Sh}}{}^{(k+n)}q_{h4,j}\uparrow\right) \\
&= {}^{k}L_{23,i}\uparrow + \sum_{j=i}^{i+m}\left(\frac{{}^{k}P_{h2,j}\uparrow}{K_{Sh}}{}^{k}q_{h2,j}\uparrow + \frac{{}^{k}P_{h3,j}\uparrow}{K_{Sh}}{}^{k}q_{h3,j}\uparrow\right) \\
&\quad + \sum_{t=k}^{k+n-1}\sum_{j=i-m+1}^{i+m-1}\left(\frac{{}^{t}P_{h2,j}\downarrow}{K_{Sh}}{}^{t}q_{h2,j}\downarrow + \frac{{}^{t}P_{h3,j}\downarrow}{K_{Sh}}{}^{t}q_{h3,j}\downarrow\right) \\
&\quad + \sum_{t=k+1}^{k+n-1}\sum_{j=i-m}^{i+m}\left(\frac{{}^{t}P_{h2,j}\uparrow}{K_{Sh}}{}^{t}q_{h2,j}\uparrow + \frac{{}^{t}P_{h3,j}\uparrow}{K_{Sh}}{}^{t}q_{h3,j}\uparrow\right) \\
&\quad + \sum_{j=i-m}^{i-1}\left(\frac{{}^{(k+n)}P_{h2,j}\uparrow}{K_{Sh}}{}^{(k+n)}q_{h2,j}\uparrow + \frac{{}^{(k+n)}P_{h3,j}\uparrow}{K_{Sh}}{}^{(k+n)}q_{h3,j}\uparrow\right)
\end{aligned}
$$

$$
\begin{aligned}
{}^{(k+n)}H_{13,i}\uparrow &= {}^{(k+n)}H_{13,i-1}\uparrow + {}^{(k+n)}\Delta_{v13,i-1}\uparrow \\
&= {}^{k}H_{13,i}\uparrow + \sum_{j=i}^{i+m}\left(\frac{{}^{k}P_{v1,j}\uparrow}{K_{Sv}}{}^{k}q_{v1,j}\uparrow + \frac{{}^{k}P_{v3,j}\uparrow}{K_{Sv}}{}^{k}q_{v3,j}\uparrow\right) \\
&+ \sum_{j=i-m+1}^{i+m-1}\left(\frac{{}^{k}P_{v1,j}\downarrow}{K_{Sv}}{}^{k}q_{v1,j}\downarrow + \frac{{}^{k}P_{v3,j}\downarrow}{K_{Sv}}{}^{k}q_{v3,j}\downarrow\right) \\
&+ \sum_{j=i-m}^{i+m}\left(\frac{{}^{(k+1)}P_{v1,j}\uparrow}{K_{Sv}}{}^{(k+1)}q_{v1,j}\uparrow + \frac{{}^{(k+1)}P_{v3,j}\uparrow}{K_{Sv}}{}^{(k+1)}q_{v3,j}\uparrow\right) \\
&+ \sum_{j=i-m+1}^{i+m-1}\left(\frac{{}^{(k+1)}P_{v1,j}\downarrow}{K_{Sv}}{}^{(k+1)}q_{v1,j}\downarrow + \frac{{}^{(k+1)}P_{v3,j}\downarrow}{K_{Sv}}{}^{(k+1)}q_{v3,j}\downarrow\right) + \ldots \\
&+ \sum_{j=i-m}^{i+m}\left(\frac{{}^{(k+n-1)}P_{v1,j}\uparrow}{K_{Sv}}{}^{(k+n-1)}q_{v1,j}\uparrow + \frac{{}^{(k+n-1)}P_{v3,j}\uparrow}{K_{Sv}}{}^{(k+n-1)}q_{v3,j}\uparrow\right) \\
&+ \sum_{j=i-m+1}^{i+m-1}\left(\frac{{}^{(k+n-1)}P_{v1,j}\downarrow}{K_{Sv}}{}^{(k+n-1)}q_{v1,j}\downarrow + \frac{{}^{(k+n-1)}P_{v3,j}\downarrow}{K_{Sv}}{}^{(k+n-1)}q_{v3,j}\downarrow\right) \\
&+ \sum_{j=i-m}^{i-1}\left(\frac{{}^{(k+n)}P_{v1,j}\uparrow}{K_{Sv}}{}^{(k+n)}q_{v1,j}\uparrow + \frac{{}^{(k+n)}P_{v3,j}\uparrow}{K_{Sv}}{}^{(k+n)}q_{v3,j}\uparrow\right) \\
&= {}^{k}H_{13,i}\uparrow + \sum_{j=i}^{i+m}\left(\frac{{}^{k}P_{v1,j}\uparrow}{K_{Sv}}{}^{k}q_{v1,j}\uparrow + \frac{{}^{k}P_{v3,j}\uparrow}{K_{Sv}}{}^{k}q_{v3,j}\uparrow\right) \\
&+ \sum_{t=k}^{k+n-1}\sum_{j=i-m+1}^{i+m-1}\left(\frac{{}^{t}P_{v1,j}\downarrow}{K_{Sv}}{}^{t}q_{v1,j}\downarrow + \frac{{}^{t}P_{v3,j}\downarrow}{K_{Sv}}{}^{t}q_{v3,j}\downarrow\right) \\
&+ \sum_{t=k+1}^{k+n-1}\sum_{j=i-m}^{i+m}\left(\frac{{}^{t}P_{v1,j}\uparrow}{K_{Sv}}{}^{t}q_{v1,j}\uparrow + \frac{{}^{t}P_{v3,j}\uparrow}{K_{Sv}}{}^{t}q_{v3,j}\uparrow\right) \\
&+ \sum_{j=i-m}^{i-1}\left(\frac{{}^{(k+n)}P_{v1,j}\uparrow}{K_{Sv}}{}^{(k+n)}q_{v1,j}\uparrow + \frac{{}^{(k+n)}P_{v3,j}\uparrow}{K_{Sv}}{}^{(k+n)}q_{v3,j}\uparrow\right)
\end{aligned}
\tag{A.3}
$$

$$
\begin{aligned}
{}^{(k+n)}H_{24,i}\uparrow &= {}^{(k+n)}H_{24,i-1}\uparrow + {}^{(k+n)}\Delta_{v24,i-1}\uparrow \\
&= {}^{k}H_{24,i}\uparrow + \sum_{j=i}^{i+m}\left(\frac{{}^{k}P_{v2,j}\uparrow}{K_{Sv}}{}^{k}q_{v2,j}\uparrow + \frac{{}^{k}P_{v4,j}\uparrow}{K_{Sv}}{}^{k}q_{v4,j}\uparrow\right) \\
&+ \sum_{j=i-m+1}^{i+m-1}\left(\frac{{}^{k}P_{v2,j}\downarrow}{K_{Sv}}{}^{k}q_{v2,j}\downarrow + \frac{{}^{k}P_{v4,j}\downarrow}{K_{Sv}}{}^{k}q_{v4,j}\downarrow\right) \\
&+ \sum_{j=i-m}^{i+m}\left(\frac{{}^{(k+1)}P_{v2,j}\uparrow}{K_{Sv}}{}^{(k+1)}q_{v2,j}\uparrow + \frac{{}^{(k+1)}P_{v4,j}\uparrow}{K_{Sv}}{}^{(k+1)}q_{v4,j}\uparrow\right) \\
&+ \sum_{j=i-m+1}^{i+m-1}\left(\frac{{}^{(k+1)}P_{v2,j}\downarrow}{K_{Sv}}{}^{(k+1)}q_{v2,j}\downarrow + \frac{{}^{(k+1)}P_{v4,j}\downarrow}{K_{Sv}}{}^{(k+1)}q_{v4,j}\downarrow\right) + \ldots \\
&+ \sum_{j=i-m}^{i+m}\left(\frac{{}^{(k+n-1)}P_{v2,j}\uparrow}{K_{Sv}}{}^{(k+n-1)}q_{v2,j}\uparrow + \frac{{}^{(k+n-1)}P_{v4,j}\uparrow}{K_{Sv}}{}^{(k+n-1)}q_{v4,j}\uparrow\right) \\
&+ \sum_{j=i-m+1}^{i+m-1}\left(\frac{{}^{(k+n-1)}P_{v2,j}\downarrow}{K_{Sv}}{}^{(k+n-1)}q_{v2,j}\downarrow + \frac{{}^{(k+n-1)}P_{v4,j}\downarrow}{K_{Sv}}{}^{(k+n-1)}q_{v4,j}\downarrow\right) \\
&+ \sum_{j=i-m}^{i-1}\left(\frac{{}^{(k+n)}P_{v2,j}\uparrow}{K_{Sv}}{}^{(k+n)}q_{v2,j}\uparrow + \frac{{}^{(k+n)}P_{v4,j}\uparrow}{K_{Sv}}{}^{(k+n)}q_{v4,j}\uparrow\right) \\
&= {}^{k}H_{24,i}\uparrow + \sum_{j=i}^{i+m}\left(\frac{{}^{k}P_{v2,j}\uparrow}{K_{Sv}}{}^{k}q_{v2,j}\uparrow + \frac{{}^{k}P_{v4,j}\uparrow}{K_{Sv}}{}^{k}q_{v4,j}\uparrow\right) \\
&+ \sum_{t=k}^{k+n-1}\sum_{j=i-m+1}^{i+m-1}\left(\frac{{}^{t}P_{v2,j}\downarrow}{K_{Sv}}{}^{t}q_{v2,j}\downarrow + \frac{{}^{t}P_{v4,j}\downarrow}{K_{Sv}}{}^{t}q_{v4,j}\downarrow\right) \\
&+ \sum_{t=k+1}^{k+n-1}\sum_{j=i-m}^{i+m}\left(\frac{{}^{t}P_{v2,j}\uparrow}{K_{Sv}}{}^{t}q_{v2,j}\uparrow + \frac{{}^{t}P_{v4,j}\uparrow}{K_{Sv}}{}^{t}q_{v4,j}\uparrow\right) \\
&+ \sum_{j=i-m}^{i-1}\left(\frac{{}^{(k+n)}P_{v2,j}\uparrow}{K_{Sv}}{}^{(k+n)}q_{v2,j}\uparrow + \frac{{}^{(k+n)}P_{v4,j}\uparrow}{K_{Sv}}{}^{(k+n)}q_{v4,j}\uparrow\right)
\end{aligned}
\tag{A.4}
$$

References

1. Slocum AH (1992) Precision machine design. Prentice Hall, Englewood Cliffs, New Jersey
2. Cui X, Zhao B, Jiao F, Zheng J (2016) Chip formation and its effects on cutting force, tool temperature, tool stress, and cutting edge wear in high- and ultra-high-speed milling. Int J Adv Manuf Technol 83(1–4):55–65
3. Gomez-Acedo E, Olarra A, Calle LNLDL (2012) A method for thermal characterization and modeling of large gantry-type machine tools. Int J Adv Manuf Technol 62(9):875–886
4. Pozo DD, Lacalle LNLD, López JM, Hernández A (2008) Prediction of press/die deformation for an accurate manufacturing of drawing dies. Int J Adv Manuf Technol 37(7–8):649–656
5. Altintas Y, Verl A, Brecher C, Uriarte L, Pritschow G (2011) Machine tool feed drives. CIRP Ann Manuf Technol 60(2): 779–796
6. Lamikiz A, Lacalle LNLD, Ocerin O, Díez D, Maidagan E (2008) The denavit and hartenberg approach applied to evaluate the consequences in the tool tip position of geometrical errors in five-axis milling centres. Int J Adv Manuf Technol 37(1–2):122–139
7. Xue F, Zhao W, Chen Y, Wang Z (2012) Research on error averaging effect of hydrostatic guideways. Precis Eng 36(1):84–90
8. ISO 230–2:(2006) Test code for machine tools. Part 2: Determination of accuracy and repeatability of positioning numerically controlled axes
9. Powałka B, Okulik T (2012) Dynamics of the guideway system founded on casting compound. Int J Adv Manuf Technol 59(1):1–8
10. Lee RS, Lin YH (2012) Applying bidirectional kinematics to assembly error analysis for five-axis machine tools with general orthogonal configuration. Int J Adv Manuf Technol 62(9–12):1261–1272
11. Mori M, Ota K, Matsubara A, Mizuyama H (2015) Design and formation of workforce skills for machine tool assembly. CIRP Ann Manuf Technol 64(1):459–462
12. Guo J, Li B, Liu Z, Hong J, Zhou Q (2016) A new solution to the measurement process planning for machine tool assembly based on kalman filter. Precis Eng 43:356–369
13. Martin P, Schneider F, Dantan JY (2005) Optimal adjustment of a machine tool for improving the geometrical quality of machined parts. Int J Adv Manuf Technol 26(5–6):559–564
14. Guo J, Liu Z, Li B, Hong J (2015) Optimal tolerance allocation for precision machine tools in consideration of measurement and adjustment processes in assembly. Int J Adv Manuf Technol 80(9–12): 1625–1640

15. Sun Y, Wang D, Dong H, Xue R, Yu S (2014) Pre-deformation for assembly performance of machine centers. Chin J Mech Eng-En 27(3):528–536
16. He G, Guo L, Li S, Zhang D (2017) Simulation and analysis for accuracy predication and adjustment for machine tool assembly process. Adv Mech Eng 9(11):168781401773447
17. Ma J, Lu D, Zhao W (2015) Assembly errors analysis of linear axis of CNC machine tool considering component deformation. Int J Adv Manuf Technol 86(1):1–9
18. Hwang J, Park CH, Kim SW (2010) Estimation method for errors of an aerostatic planar XY stage based on measured profiles errors. Int J Adv Manuf Technol 46(9–12):877–883
19. Khim G, Park CH, Shamoto E, Kim SW (2011) Prediction and compensation of motion accuracy in a linear motion bearing table. Precis Eng 35(3):393–399
20. Tang H, Duan JA, Zhao Q (2017) A systematic approach on analyzing the relationship between straightness & angular errors and guideway surface in precise linear stage ☆. Int J Mach Tools Manuf 120:12–19
21. Majda P (2012) Modeling of geometric errors of linear guideway and their influence on joint kinematic error in machine tools. Precis Eng 36(3):369–378
22. Wu J, Wang J, Wang L, Li T, You Z (2009) Study on the stiffness of a 5-DOF hybrid machine tool with actuation redundancy. Mech Mach Theory 44(2):289–305